

Large-Scale Conformational Dynamics Control H5N1 Influenza Polymerase PB2 Binding to Importin α

Elise Delaforge,^{†,‡,§} Sigrd Milles,^{†,‡,§} Guillaume Bouvignies,^{†,‡,§} Denis Bouvier,^{†,‡,§,||,⊥,♯} Stephane Boivin,^{||,⊥,♯} Nicola Salvi,^{†,‡,§} Damien Maurin,^{†,‡,§} Anne Martel,[¶] Adam Round,[□] Edward A. Lemke,[△] Malene Ringkjøbing Jensen,^{†,‡,§} Darren J. Hart,^{*,||,⊥,♯} and Martin Blackledge^{*,†,‡,§}

[†]Univ. Grenoble Alpes, Institut de Biologie Structurale (IBS), F-38044 Grenoble, France

[‡]CEA, DSV, IBS, F-38044 Grenoble, France

[§]CNRS, IBS, F-38044 Grenoble, France

^{||}Univ. Grenoble Alpes, UVHCI, Grenoble, France

[⊥]CNRS, UVHCI, Grenoble, France

[♯]Unit for Virus Host Cell Interactions, Univ. Grenoble Alpes-EMBL-CNRS, Grenoble, France

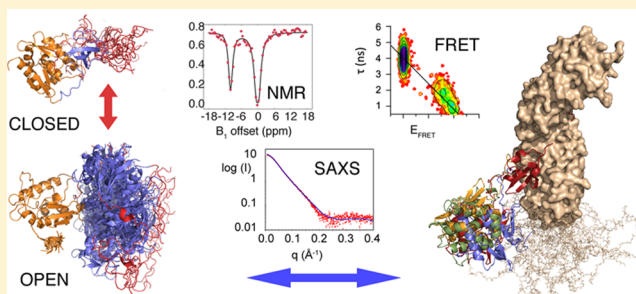
[¶]Institut Laue-Langevin, F-38044 Grenoble, France

[□]European Molecular Biology Laboratory, Grenoble Outstation, 38042 Grenoble, France

[△]European Molecular Biology Laboratory, Structural and Computational Biology Unit, Meyerhofstrasse 1, 69117 Heidelberg, Germany

Supporting Information

ABSTRACT: Influenza A RNA polymerase complex is formed from three components, PA, PB1, and PB2. PB2 is independently imported into the nucleus prior to polymerase reconstitution. All crystallographic structures of the PB2 C-terminus (residues 536–759) reveal two globular domains, 627 and NLS, that form a tightly packed heterodimer. The molecular basis of the affinity of 627-NLS for importins remained unclear from these structures, apparently requiring large-scale conformational changes prior to importin binding. Using a combination of solution-state NMR, small-angle neutron scattering, small-angle X-ray scattering (SAXS), and Förster resonance energy transfer (FRET), we show that 627-NLS populates a temperature-dependent dynamic equilibrium between closed and open states. The closed state is stabilized by a tripartite salt bridge involving the 627-NLS interface and the linker, that becomes flexible in the open state, with 627 and NLS dislocating into a highly dynamic ensemble. Activation enthalpies and entropies associated with the rupture of this interface were derived from simultaneous analysis of temperature-dependent chemical exchange saturation transfer measurements, revealing a strong temperature dependence of both open-state population and exchange rate. Single-molecule FRET and SAXS demonstrate that only the open-form is capable of binding to importin α and that, upon binding, the 627 domain samples a dynamic conformational equilibrium in the vicinity of the C-terminus of importin α . This intrinsic large-scale conformational flexibility therefore enables 627-NLS to bind importin through conformational selection from a temperature-dependent equilibrium comprising both functional forms of the protein.



INTRODUCTION

Influenza A viruses are a major concern for human health, causing both annual epidemics and less frequent pandemics. Influenza A is a member of the Orthomyxoviridae family, with a segmented genome that comprises eight negative-sense RNA strands, encoding 10 major proteins and 5 auxiliary polypeptides.¹ The eight negative-polarity RNA genomic segments are each complexed with many copies of the nucleoprotein (NP) and one copy of the viral polymerase, forming the viral RNP that is packaged into a membrane-enveloped viral particle.^{2–5} The RNA polymerase complex

comprises three subunits: PA (acidic protein), PB1 (basic protein 1), and PB2 (basic protein 2). Following infection of the host cell, the RNP is imported into the nucleus where it performs the first cycle of transcription. The resulting viral mRNAs are translated in the cytoplasm to produce new viral proteins, of which PB2⁶ and the PA–PB1⁷ heterodimer are imported into the nucleus where they assemble into new

Received: July 24, 2015

Published: October 1, 2015

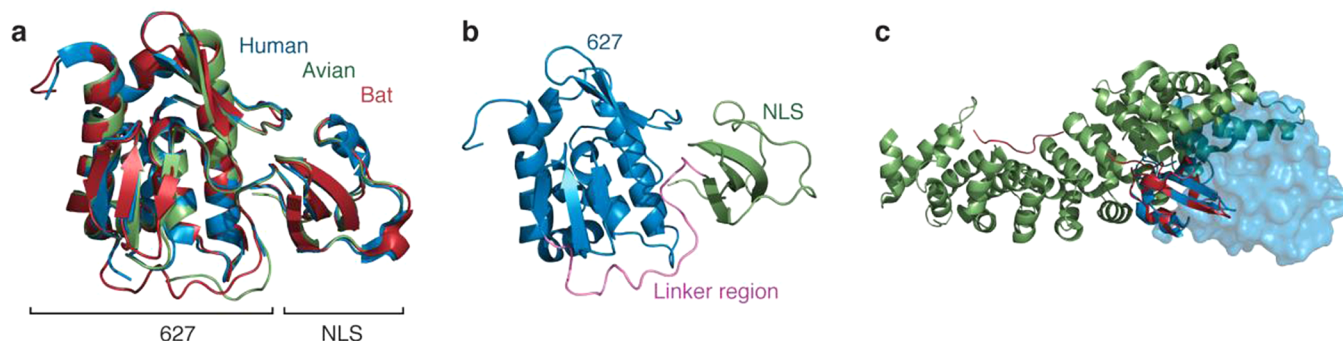


Figure 1. Crystallographic structure of 627-NLS is incompatible with importin binding. (a) Superposition of the crystal structures of 627-NLS of influenza A from human (PDB 2VY6, blue), avian (this work, green) together with the domain from bat influenza virus present in full heterotrimeric polymerase (PDB 4WSB, red). (b) Crystal structure of bat 627-NLS showing the linker peptide (magenta) connecting the 627 and NLS domains. (c) Crystal structure of human importin $\alpha 5$ (green) in complex with NLS (red) (PDB 2JDQ). Superposition of the human 627-NLS structure (blue) on the importin:NLS structure reveals a steric clash between importin and the 627 domain (transparent blue surface).

functional polymerase heterotrimers that catalyze further rounds of viral RNA replication and transcription.

The C-terminus of PB2 comprises two domains, the 627 (residues 538–677) and the NLS (residues 689–759) domains, showing negligible sequence or structural similarities with known proteins.^{6,8} The linear nuclear localization signal (NLS) peptide, located at the C-terminus of 627-NLS interacts with importin α *in vivo*, resulting in transfer of PB2 to the nucleus. Insight into the structural basis of the interaction of 627-NLS with importin α was initially obtained from the structure of the NLS domain free and in complex with importin $\alpha 5$,⁶ showing how the bipartite NLS peptide 736-RKRX₁₂KRIR-755 binds importin α . The structure of a construct comprising both 627 and NLS (residues 538–759) revealed a single well-packed conformation (Figure 1), although both domains are stable and soluble separately.^{6,9} The recent determination of the structure of bat influenza A polymerase complex, comprising subunits PA, PB1, and PB2, bound to its viral RNA promoter, revealed identical quaternary structure of these two PB2 domains within the context of the functional polymerase, where 627-NLS constitutes part of the putative basic exit channel for capped transcript RNA.¹⁰

Adaptation of avian viruses to human hosts is characterized by accumulation of mutations, especially in the PB2 C-terminal region comprising the 627-NLS domain, where surface residues exhibit positively charged clusters.^{9,11} Temperature-dependent replication has been observed¹² in line with adaptation of the viral proteins from the warmer environment of the bird intestine to the cooler mammalian respiratory tract, but the molecular basis of this effect is unknown. There is however evidence that mutations in this region directly modulate importin binding,^{13,14} while variations in the NLS peptide sequence have been shown to disrupt active polymerase assembly suggesting a second chaperone-like role for importins.¹⁵

Studying the interaction of 627-NLS with importin is therefore crucial to understanding the mechanistic role of this domain in nuclear import. The interaction is particularly intriguing since attempts to model the complex on the basis of the 627-NLS and NLS:importin $\alpha 5$ crystal structures predict a severe steric clash between the 627 domain and importin (Figure 1c), although 627-NLS binds importin with similar affinity to the NLS domain alone.¹⁶ These observations suggest that large scale conformational changes in importin or 627-NLS are necessary to allow formation of the complex in solution.

In the current study we investigate the molecular basis of the interaction between 627-NLS from avian influenza and importin $\alpha 1$ in solution using nuclear magnetic resonance (NMR), small-angle X-ray scattering (SAXS), and single-molecule Förster resonance energy transfer (smFRET). These complementary methods reveal the coexistence of two very different conformations of 627-NLS in solution corresponding to open and closed states. The two forms interchange in a highly dynamic equilibrium with a slow characteristic exchange rate ($k_{\text{ex}} = 30 \text{ s}^{-1}$ at 15 °C). The closed form is stabilized by a tripartite salt bridge in the interface, implicating highly conserved basic and acidic amino acids in the 627 and NLS domains and the inter-domain linker.⁹ Mutation of one of these amino acids results in suppression of the closed form in solution. The population of the open form, in which the NLS domain is free to interact with importin, increases as temperature increases toward the physiological range. Analysis of the 627-NLS:importin complex using SAXS and smFRET shows that 627-NLS adopts an open conformation when binding importin, with the 627 domain remaining flexible on the surface of importin. These observations therefore present a structural, dynamic, and thermodynamic paradigm for understanding how the C-terminal region of PB2 interacts with importin and how the polymerase subunit is shuttled into the nucleus, identifying a role for conformational selection from a pre-existing equilibrium, and suggesting a possible role for temperature regulation of this essential equilibrium during inter-species adaptation.

RESULTS

627-NLS Exchanges between Open and Closed Conformations in Solution. We have determined the crystalline structure of 627-NLS from avian H5N1 influenza virus, which is found to be very similar (backbone rmsd 0.4 Å) to the previously determined human form,⁹ and the recently determined bat influenza B 627-NLS from the complete polymerase complex (Figure 1a)¹⁰ as well as other known 627-NLS structures.^{8,17,18} In most crystal structures it is possible to trace part or all of the peptide linking the two domains (residues 674–693), revealing strong similarity of the visible parts of the linker in human and avian forms (Figure 1b). As shown previously for human 627-NLS,⁹ superposition of the structure of avian 627-NLS with the NLS:importin $\alpha 5$ ⁶ structure via their common NLS domain results in a significant clash between the 627 domain and the C-terminal region of

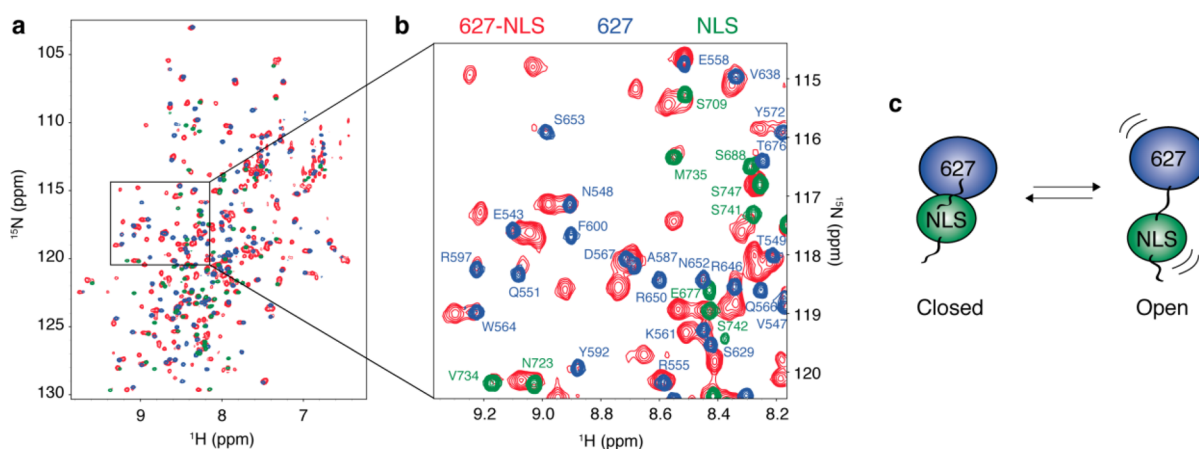


Figure 2. 627-NLS samples an equilibrium between closed and open conformations. (a) Comparison of ^1H – ^{15}N TROSY spectra of avian 627-NLS (red), 627 (blue), and NLS (green) at 25 °C. (b) Expanded region of the spectra displayed in (a) with assignments shown for the two separate domains 627 and NLS. (c) 627-NLS populates a dynamic equilibrium of closed and open conformations in slow exchange on the NMR chemical shift time scale.

importin α ,¹⁶ indicating that the conformation observed in the crystal structure is not binding-competent (Figure 1c). Attempts to crystallize the 627-NLS:importin complex were also unsuccessful (data not shown). Based on highly similar NLS-domain-bound structures of importin $\alpha 1$, $\alpha 3$, $\alpha 7$,¹⁹ and $\alpha 5$,⁹ identical clashes would be predicted with the 627 domain, although all isoforms have been shown to import PB2 *in vivo*,²⁰ including importin $\alpha 1$ studied here.¹³

To resolve this issue, we have investigated the conformational behavior of avian 627-NLS in solution using high-resolution NMR spectroscopy. Remarkably, ^1H – ^{15}N transverse relaxation optimized spectroscopy (TROSY) spectra of 627-NLS at 25 °C show around 350 peaks corresponding to backbone amides (Figure 2a), where only 213 are expected, indicating a conformational exchange of the protein on a slow NMR time scale. Comparison of TROSY spectra of isolated 627 and NLS domains with the spectrum of 627-NLS, shows a near-perfect superposition of the vast majority of resonances of 627 and NLS with one set of the 627-NLS resonances (Figure 2b). Assignment of the 627 and NLS domains and the two sets of peaks in the 627-NLS construct (Tables S1–S3) allows comparison of ^{13}C chemical shifts, demonstrating that the secondary structures of both sets of peaks are highly similar and largely coincident with that of the crystal structure (Figure 3a and Figure S1). Nearly all significant deviations localized to the linker region. ^{15}N chemical shifts are more sensitive to the local environment, and comparison of these shifts in the two forms maps predominantly to the interface between the two domains as well as the linker (Figure 3b,c and Figure S1d).

On the basis of these observations, we propose that 627-NLS undergoes slow exchange between a closed form, most likely the conformation found in the crystal lattice, and an open form in which the linker becomes flexible, and the two sub-domains, while retaining secondary and tertiary structure, dislocate and evolve more or less independently (Figure 2c). The open state is therefore highly dynamic, rapidly sampling the extensive degrees of conformational freedom allowed by the linker peptide, on a time scale that is fast enough to give rise to a single set of narrow NMR resonances ($\tau_{\text{ex}} < 50 \mu\text{s}$). We note that a similar behavior is observed for the human 627-NLS domain, which also displays sets of resonances corresponding to closed and open conformations (Figure S1e).

The Closed Form of 627-NLS Is Stabilized by a Tripartite Salt Bridge. Examination of the crystal structure of avian, human, and bat 627-NLS identifies a tripartite salt bridge in the interface between the two domains (Figure 4a), implicating a basic side chain from the 627 domain (R650) an acidic side chain from the NLS domain (D730), and an acidic side chain from the linker peptide (E687). This configuration is conserved in all available crystal structures of 627-NLS from different strains of influenza A and B,^{8–10,17,18} as is the presence of acidic and basic side chains at these positions (Figure S2). The implication of the linker peptide in this stabilizing interaction, resulting in structuring of the peptide and an uncommon insertion of the linker into the inter-domain interface, explains why this region of the peptide is structured and partially or fully resolved in the different crystal structures. A mutation of R650 to an alanine (R650A) removes all visible evidence of the closed form on the basis of NMR spectroscopy, with the only remaining peaks coinciding with the resonances of the individual domains (and therefore the open form) (Figure 4b). Spin relaxation demonstrates that the linker peptide (residues 676–689) of 627-NLS exhibits increased dynamics (Figure 4c), while the two domains present differential rotational correlation properties, related to their different molecular dimensions (130 compared to 60 amino acids) as determined from transverse auto- and cross-correlated relaxation rates (Figure S3). We note that the specific exchange regime characterizing the interchange between open and closed forms severely complicates interpretation of relaxation rates measured in wild-type protein due to averaging of dynamic characteristics of the open and closed states.

Equilibrium between Open and Closed 627-NLS Conformations Is Temperature-Dependent. We have used NMR spectroscopy to investigate the temperature dependence of the equilibrium between open and closed conformations. TROSY spectra of ^{15}N -labeled avian 627-NLS at 5, 10, 15, 20, 25, 30, and 35 °C were recorded. As temperature increases, the intensity of signals corresponding to the open conformation increases while that of the closed conformation decreases (Figure 5a). A representative sample of residues displaying well-resolved peaks, corresponding to open and closed conformations were quantified using a line shape analysis at the different temperatures, resulting in a population

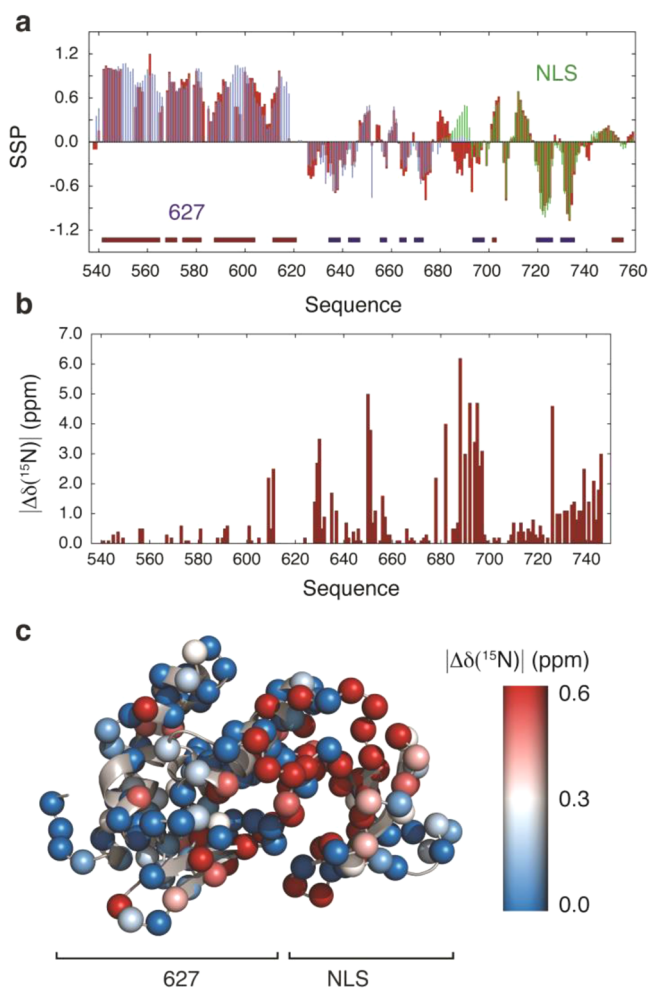


Figure 3. Chemical shift differences between individual domains and 627-NLS. (a) Secondary structure propensities (SSP) of 627 (blue, 25 °C), NLS (green, 25 °C), and 627-NLS (red, 10 °C) calculated from experimental $^{13}\text{C}\alpha$ and $^{13}\text{C}\beta$ chemical shifts.⁶⁷ The chemical shifts of 627 were obtained using a deuterated sample, while the chemical shifts of 627-NLS were obtained using a perdeuterated sample. Corrections were made for isotope effects on experimental chemical shifts of perdeuterated 627-NLS using the corrections recently published by Maltsev et al.⁶⁸ In the case of 627-NLS, the SSP score is reported for the set of resonances corresponding to the closed form of 627-NLS or, if applicable, the resonances where the open and closed forms are indistinguishable. Horizontal bars in the bottom panel indicate the position of helices (red bars) and sheets (blue bars) as observed in the crystal structure of avian 627-NLS. (b) ^{15}N chemical shift differences between the resonances corresponding to open and closed conformations as a function of the sequence of 627-NLS. (c) ^{15}N chemical shift differences mapped onto the crystallographic structure of 627-NLS showing that the largest shifts correspond to the crystallographic interface between 627 and NLS.

shift from predominantly closed at 10 °C to approximately equal populations at 30 °C (Figure 5c). Chemical exchange saturation transfer (CEST)²¹ experiments were used to examine the conformational equilibrium in more detail, providing a precise determination of the variation of the exchange rate and population with temperature (Figure 5c,d). Activation enthalpies and entropies associated with breaking the stabilizing interface between the domains (Table 1) were derived from simultaneous analysis of CEST data from a series of eight well-resolved resonances corresponding to the closed

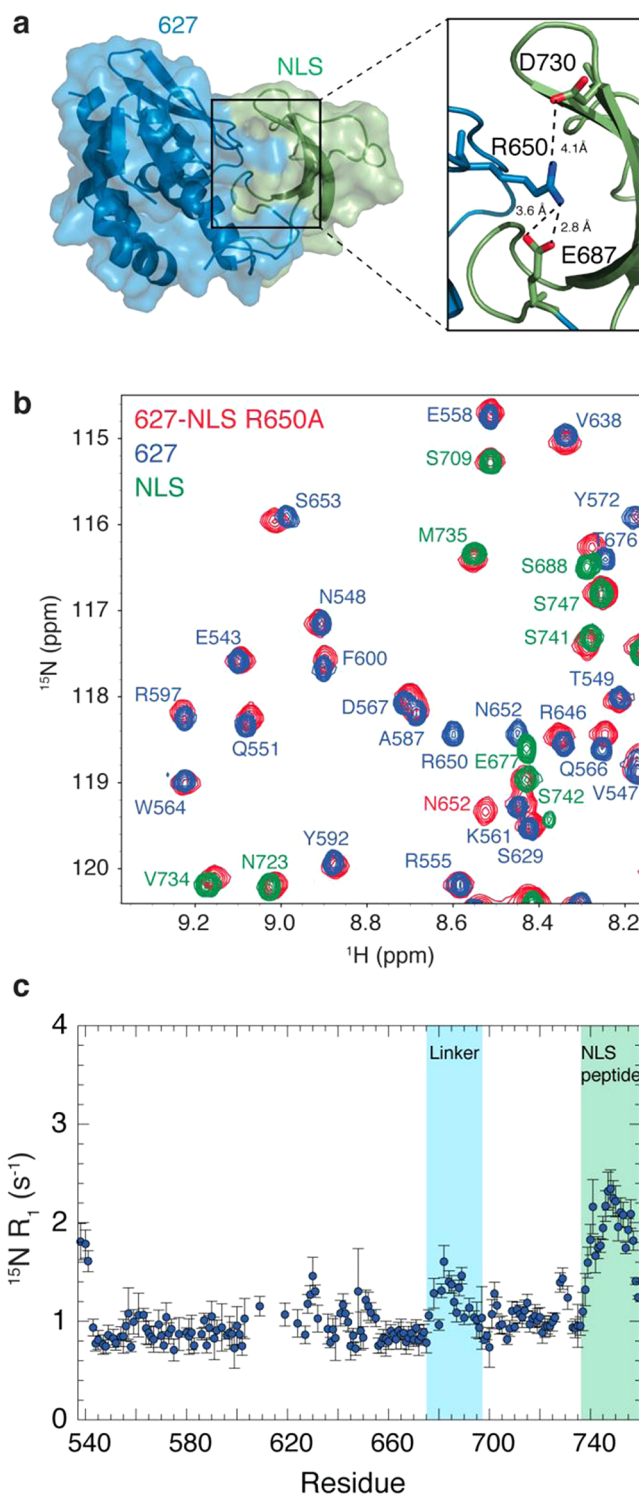


Figure 4. A salt bridge stabilizes the closed conformation of 627-NLS. (a) Crystal structure of avian 627-NLS showing that R650 stabilizes the closed conformation of 627-NLS via interactions with E687 of the linker region and D730 of the NLS domain. (b) Expanded region of the ^1H - ^{15}N TROSY spectra of 627-NLS R650A (red), 627 (blue), and NLS (green) obtained at 25 °C. (c) ^{15}N R_1 relaxation rates of 627-NLS R650A at a ^1H frequency of 600 MHz and 10 °C.

state of 627-NLS at temperatures ranging from 5 to 20 °C (two resonances reporting on residues from either the 627 or NLS domains are shown in Figure 5b) assuming an Eyring relationship (see Methods). All individual CEST traces are

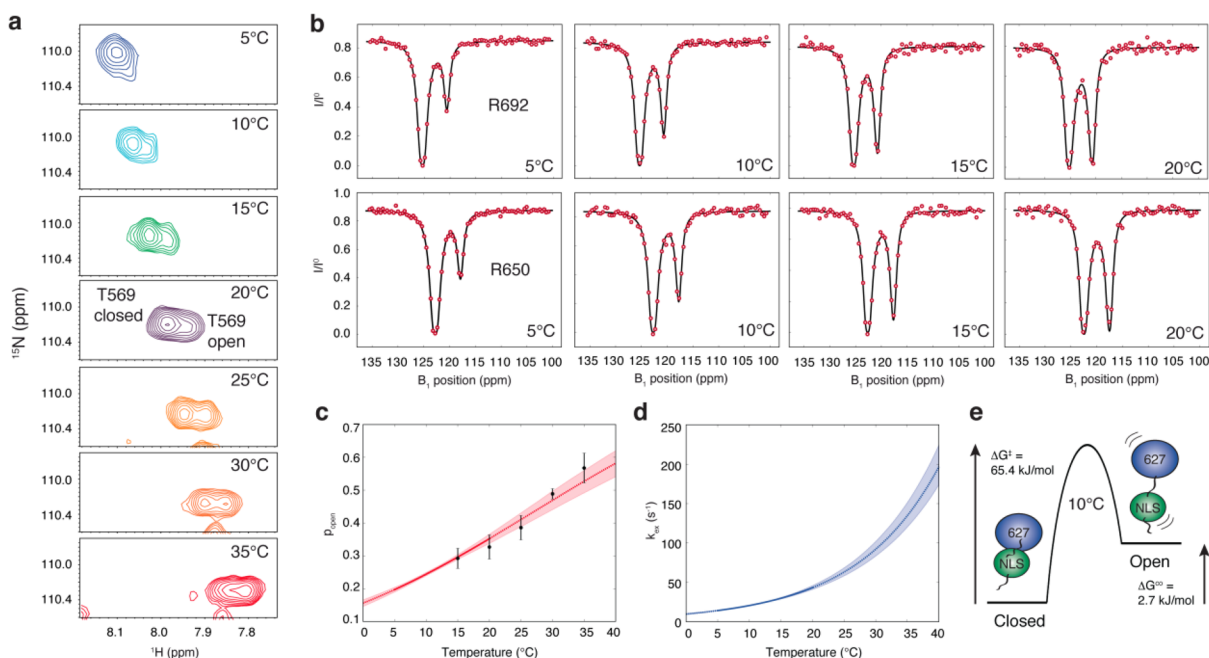


Figure 5. Characterization of the conformational exchange between open and closed conformations of 627-NLS. (a) Expanded regions of the ^1H - ^{15}N TROSY spectra of 627-NLS at multiple temperatures showing two resonances corresponding to open and closed conformations of the amide group of T569. (b) Experimental ^{15}N CEST profiles (red points) for the residues R692 and R650 obtained at multiple temperatures. The black lines correspond to a fit to a two-site exchange model by analyzing simultaneously data for multiple selected residues (Figure S4) at 5, 10, 15, and 20 °C assuming an Eyring relationship. (c) Population of open conformation (p_{open}) as a function of temperature derived from a line shape analysis of TROSY spectra at different temperatures (black points) or extracted from CEST experiments (red line). The full-drawn red line indicates the temperature range where CEST experiments were recorded. The shaded red area shows the 68% confidence interval as obtained by 500 Monte Carlo simulations. (d) Exchange rate (k_{ex}) between open and closed conformations of 627-NLS obtained from CEST experiments (blue line). The full-drawn blue line indicates the temperature range where CEST experiments were recorded. The shaded blue area shows the 68% confidence interval as obtained by 500 Monte Carlo simulations. (e) Schematic representation of the energy diagram of the open and closed states of 627-NLS at 10 °C with ΔG values derived from CEST experiments (see Methods).

Table 1. Thermodynamic Parameters of the Conformational Equilibrium between Open and Closed Conformations of 627-NLS Derived from CEST Experiments Recorded at Four Different Temperatures^a

	ΔH (kJ mol ⁻¹)	ΔS (J mol ⁻¹ ·K ⁻¹)	$\Delta G_{10\text{ }^\circ\text{C}}$ (kJ mol ⁻¹)
energies of open state	36 ± 4	117 ± 15	2.66 ± 0.06
energies of activation	74 ± 2	32 ± 7	65.44 ± 0.02

^aRecorded at 5, 10, 15, and 20°C. The CEST experiments were analyzed simultaneously at all temperatures by including experimental data for selected residues (Figure S4) and assuming an Eyring relationship (see Methods). Energy values are reported relative to the energy of the closed state.

remarkably well reproduced using this simple model (Figure S4). Not surprisingly, the activation energy required to rupture the interactions in the interface (65 kJ/mol at 10 °C), is largely dominated by enthalpic contributions, while the free energy difference of the open compared to the closed state (2.67 kJ/mol at 10 °C) reports on dominant enthalpic contributions at lower temperatures that are matched by entropic effects as temperature increases (Figure 5e). Overall these results provide an unambiguous description of the thermodynamic origin of the increase of the exchange rate and open-state population with temperature. We note that the population dependence coincides very closely with the values derived from line shape analysis (Figure 5c). Additional CEST-based analyses were performed using human 627-NLS, the more common partner of importin $\alpha 1$ but which shows higher levels of instability *in*

vitro compared to the avian form, resulting in population and exchange rate dependences that were identical within experimental uncertainty (data not shown).

SAXS Measurements Confirm the Temperature Dependence of the Equilibrium. Open and closed forms were further characterized using SAXS. Data were collected for avian 627-NLS at concentrations of 4.9, 2.45, and 1.23 mg/mL and over a temperature range from 5 to 30 °C. Profiles obtained at different protein concentrations exhibited the same shape and were flat at low q values, indicating the absence of aggregation (Figure 6a). The radius of gyration, R_g , values derived from the Guinier approximation at low q value exhibited clear temperature dependence, with higher R_g at higher temperatures (Figure 6a). SAXS curves were simulated for the closed conformation and the open state using the *flexible-meccano* statistical coil description^{22,23} for the linker region and the CRYSOLE²⁴ algorithm for prediction of scattering profiles. Combination of these limiting curves in proportions coincident with those determined using NMR spectroscopy (CEST) results in excellent reproduction of the experimental SAXS curves obtained at the limiting temperatures (5 and 30 °C) (Figure 6b,c).

The Open Conformation of 627-NLS Binds Importin $\alpha 1$. The 627-NLS:importin $\alpha 1$ complex was investigated using small angle scattering. SAXS profiles from the complex were analyzed using two procedures. First, *flexible-meccano* was used to sample the conformational space available to the 627 domain, assuming that the linker peptide (residues 676–689) can sample all statistical coil conformations available to this

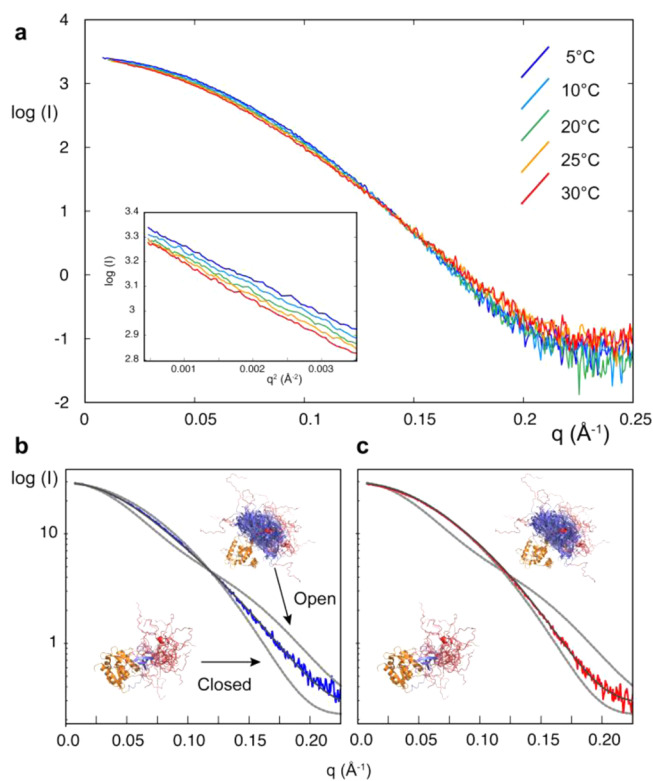


Figure 6. Small-angle X-ray scattering from 627-NLS in solution. (a) Temperature dependence of SAXS curves of the same 627-NLS sample measured at 5, 10, 20, 25, and 30 °C. Inset: Guinier region of the SAXS curve plotted as $\log_e(I)$ vs q^2 , showing that the slope gets steeper in this region as temperature increases. The extracted radii of gyration are 20.4, 20.8, 21.1, 21.3, and 21.7 Å for 5, 10, 20, 25, and 30 °C, respectively. (b,c) Comparison of experimental SAXS data to an admixture of scattering curves calculated using Crysol for the closed form and averaged over an open ensemble calculated using *flexible-meccano* (limiting curves shown in gray). The ratios of open and closed curves were taken from the populations determined from NMR line shape and CEST analyses: (b) 0.2:0.8 at 5 °C and (c) 0.5:0.5 at 30 °C.

peptide sequence. Conformations were built onto the X-ray crystal structure of the NLS domain bound to importin $\alpha 1$, assuming that the NLS domain, whose conformation is conserved in all four complexes with importin, retains this crystallographic position, an assumption supported by mutagenesis and crystallographic studies.¹⁹ SAXS curves were predicted from each of these 25 000 conformers. Note that the reproduction of experimental data by individual curves provides significant improvement over the average of all curves, indicating that the sterically available conformational space is not sampled uniformly. Conformers were then ranked with respect to their ability to reproduce the experimental SAXS curves (Figure 7a), revealing that all high-ranking solutions are positioned near the C-terminal end of importin (Figure 7b). The data reproduction derived from this procedure is already of high quality (Figure 7d); nevertheless, sub-ensembles of conformers may be selected from all possible available positions (Figure 7a), thereby accounting explicitly for the flexibility of 627 relative to NLS-importin. Not surprisingly this approach results in ensembles with a high density of states in the same region of three-dimensional space relative to importin as the single-conformation solutions (Figure 8).

Single-conformer and ensemble solutions that best reproduce the experimental SAXS curve also provide a significantly better

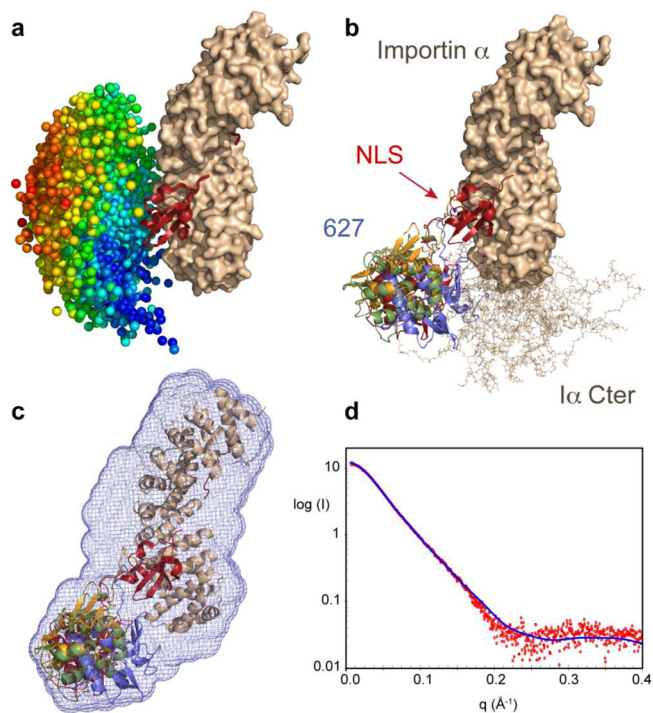


Figure 7. Structural analysis of the 627-NLS:importin $\alpha 1$ complex from small-angle X-ray scattering. (a) Representative depiction of the 25 000 centers-of-mass of different conformers of 627-NLS calculated using the *flexible-meccano* statistical coil algorithm to model the conformational space available to the 627 domain when the NLS domain is bound to importin. The center-of-mass spheres are colored with respect to the ability of the associated conformation to reproduce experimental SAXS data: red, $\chi > 4$; yellow, $4 > \chi > 3$; green, $3 > \chi > 2$; light blue, $2 > \chi > 1$; and dark blue, $\chi < 1$. (b) Representative conformations of 627 that best reproduce the experimental data are shown in cartoon representation. The position of the C-terminal disordered tail of importin $\alpha 1$ is also shown. (c) Comparison of the position of the best-fitting conformations with the *ab initio* SAXS envelope determined using DAMMIF and DAMAVER (blue). (d) Comparison of experimental SAXS data (red) with scattering profile predicted from the best fitting conformation (blue).

reproduction of independently measured small-angle neutron scattering (SANS) data (hydrogenated protein in buffer containing 100% D₂O) than the average over all conformational space (Figure S5). Under these conditions, SANS data report more faithfully on the scattering properties of the proteins alone,^{25,26} whereas SAXS data report on a combination of the solvent shell and the protein, making the two sources of information complementary and thereby further substantiating the model of the complex.

Second, an *ab initio* reconstruction was performed using DAMMIF²⁷ to produce a space-filling envelope of the scattering object. Although some empty density can be seen in this model, possibly due to flexibility of either importin $\alpha 1$ or the 627 domain, the envelope encompasses very well the single conformation solutions derived from broad sampling of conformational space, showing good overall agreement of the two approaches (Figure 7c).

smFRET Analysis of the Dynamic Properties and Importin α Binding Mode of 627-NLS. The conformational equilibria sampled in the free and bound forms of 627-NLS were also investigated by smFRET, using a double-cysteine mutant of 627-NLS (residues 539 and 707, positioned at either

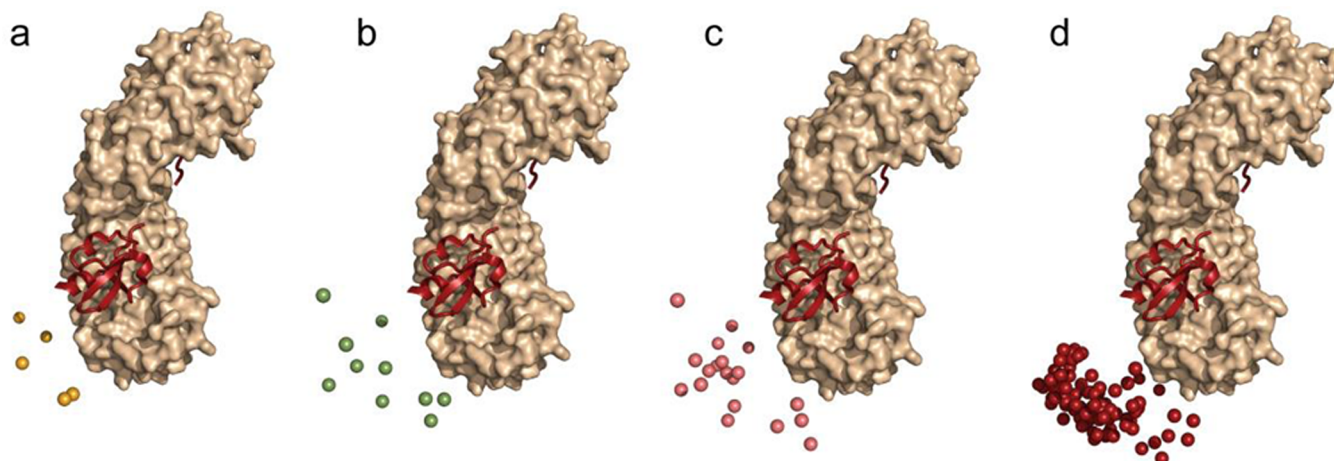


Figure 8. Ensemble selections of the 627-NLS:importin α 1 complex. Comparison between centers-of-mass of the 627 domain in ASTEROIDS-selected ensembles of 627-NLS-importin α 1 containing (a) 5, (b) 10, (c) 20, and (d) the 100 conformers presenting the lowest χ^2 of individual conformations against the experimental data. The ensembles shown in (a-c) were selected from the entire 25000 orientations represented in Figure 7a.

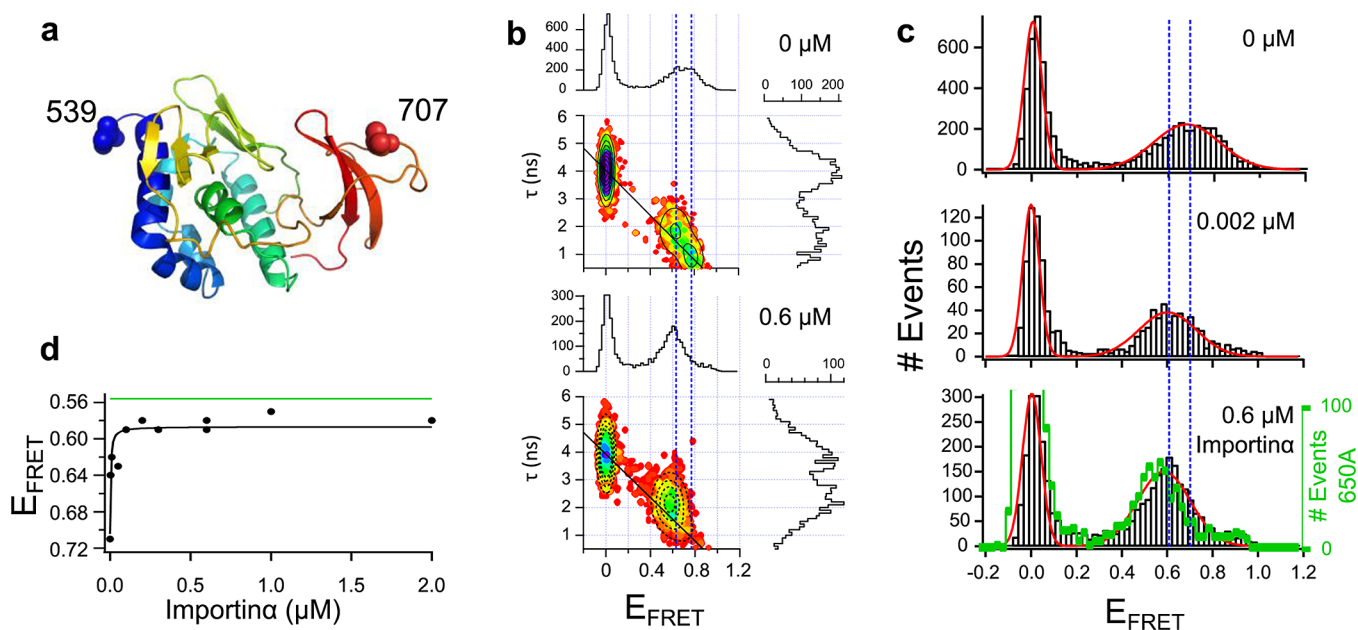


Figure 9. 627-NLS interaction with importin α 1 probed by smFRET. (a) Structure of 627-NLS with labeling sites marked as spheres. (b) Donor fluorescence lifetime (τ) versus FRET efficiency histograms of 627-NLS double-cysteine mutant I539C A707C in the presence and absence of 0.6 μ M importin α 1 with corresponding two-dimensional triple-Gaussian fits (black dashed curves) and the black line describing the relationship between τ and E_{FRET} for a static molecule. The blue dashed lines are centered at the FRET efficiencies of open and closed conformations of the unbound state. (See Figure S7 for the triple Gaussian fits of the corresponding titration.) (c) Typical one-dimensional E_{FRET} histograms of 627-NLS double-cysteine mutant I539C A707C at varying importin α 1 concentrations with corresponding Gaussian fits (red curves). The blue dashed lines illustrate E_{FRET} at 0 μ M (right) and 0.6 μ M importin α 1 (left). The green histogram stems from 627-NLS R650A I539C A707C. The histogram at 0 μ M importin α 1 was accumulated from four independent measurements. (d) E_{FRET} as obtained from a titration of 627-NLS I539C A707C with importin α 1. Fitted values (black spheres) were obtained from double Gaussian fits of two-dimensional E_{FRET} versus τ histograms, allowing a tilt between the E_{FRET} and τ axes within one population (Figure S6). E_{FRET} relation with importin α 1 concentration was described using a simple binding model, $[AB] = A_{\text{tot}}B/(K_d + B)$ + offset, where A is 627-NLS and B is importin α 1, under the assumption that importin α 1 was added at large excess at every titration step (black line). The green line illustrates E_{FRET} as obtained from 627-NLS R650A double-cysteine mutant I539C A707C.

extreme of the closed 627-NLS structure) randomly labeled with Alexa488 and Alexa594 (Figure 9a). 627-NLS was subjected to multi-parameter smFRET analysis^{28,29} and yielded a donor (Do, Alexa488)-only population, which lacked active acceptor (Ac, Alexa594) fluorophores, at a FRET efficiency (E_{FRET}) of 0, as well as a FRET population (E_{FRET}) reporting on distance and dynamics between Do and Ac. Quantitative analysis of the width of the FRET population (Table S4)

together with fluorescence lifetime (τ , Figure S6) and observation time analysis (Figure S7) points toward the existence of more than one conformation that is underlying the FRET peak (see Methods for a more detailed description).^{30–32} This is in agreement with the existence of open and closed states in 627-NLS and an exchange rate between these states (50 s^{-1} at 25 $^{\circ}\text{C}$, as determined by NMR) that is significantly slower than the average single-molecule

observation time (up to ~ 5 ms). It is likely therefore that the FRET population in the unbound state is built up from these two states. Following this logic, fitting of the E_{FRET} versus τ histogram with a triple Gaussian function (one Gaussian describing the Do-only population, two describing the FRET population) results in average $E_{\text{FRET}} = 0.62$ and 0.77 (Figure 9b,c). With an approximate dye-to-dye distance of 47 \AA , the molecules giving rise to $E_{\text{FRET}} = 0.77$ likely reflect the closed conformation of 627-NLS as observed in the crystal structure (44 \AA C α –C α distance), and behave similarly to static molecules, as can be seen from the corresponding E_{FRET}/τ relationship that follows the “static FRET line” (Figure 9b). Although we do not resolve quantitative modes of 627-NLS dynamics^{28,32,33} from these data, we observe that molecules in the open state, giving rise to $E_{\text{FRET}} = 0.62$, deviate from static behavior,^{31,32} indicating sub-microsecond averaging of different conformations within this state. The two states, open and closed, are occupied with a similar number of molecules at the smFRET temperature of $23 \text{ }^\circ\text{C}$, approximately reflecting the occupancy ratios observed by NMR (45:55 compared to 40:60 from NMR). NMR and smFRET are therefore shown to be highly complementary; while NMR provides a clear separation of time scales of interconversion between conformers in the open-form, and between the open and closed states, smFRET can be used to probe the distance distribution functions present within the two states.

When importin α was added, the FRET population shifted gradually to lower FRET efficiencies (longer distances) in agreement with an increase in the open conformation when compared to the unbound form of the 627-NLS domain (Figure 9c,d and Figure S6). A fit of the corresponding τ versus E_{FRET} histograms with a triple Gaussian function, as was done for the unbound 627-NLS (Figure 9b), suggests that the closed form gradually disappears from the distribution, substantiating the suggestion, obtained from SAXS, that only the open form is capable of binding importin (Figure 9b, Figure S7, and Table S5). It is striking that, even in the bound form, the events coming from the 627-NLS open conformation deviate from the static FRET line, indicating that 627-NLS remains flexible when bound (Figure 9b).

Single-molecule FRET of the R650A mutant confirms that the closed form is barely detectable in the ensemble in the absence of the stabilizing salt bridge, leading to slightly more extended distances compared to the open form measured in the native protein (Figure 9c and Figure S6). Single-molecule FRET on 627-NLS in the presence $5 \mu\text{M}$ importin $\alpha 3$, $\alpha 5$, and $\alpha 7$ gave effectively identical results to those found for importin $\alpha 1$, again revealing an undetectably low population of the closed form of 627-NLS, and very similar FRET efficiencies for the open form (Figure S8). This suggests the 627-NLS binding mode detected for importin $\alpha 1$ is indeed general across the importin α family.

DISCUSSION

Although the three-dimensional structure of influenza virus polymerase has recently been determined to atomic resolution,¹⁰ the molecular basis of import into the nucleus of the constituent PB2 subunit prior to reconstitution of the functional polymerase remains poorly understood. The C-terminal 627-NLS region of influenza PB2 polymerase is crucial for this interaction, as it is terminated by the NLS peptide that interacts with nuclear import receptors. This domain also contains a high density of mutations that are important for

inter-species transmission, suggesting that nuclear import may play an important role in adaptation. Here we have determined the crystal structure of a fully avian HSN1 627-NLS domain that is essentially indistinguishable from human 627-NLS and from the structure of bat influenza 627-NLS in the context of the full-length polymerase. In all available structures^{8–10,17,18} 627-NLS is stabilized in a compact conformation by a tripartite salt bridge, implicating charged amino acids in the interface between the two domains, and a third amino acid in the peptide linking the independently folded domains. On the basis of the crystal structure of the NLS domain in complex with importin, it was previously predicted that this closed conformation could not bind importin α unless 627-NLS or importin α undergo large scale conformational changes that may be further implicated in active trimeric polymerase assembly.¹⁶

Multi-domain proteins comprise 80% of eukaryotic proteomes, where inter-domain dynamics play key roles in a multitude of molecular recognition, transport, and signaling processes.³⁴ These complex dynamic modes cannot be understood from static structures of either the entire protein or individual domains. Indeed intrinsically disordered linkers connecting folded subunits often encode the degrees of conformational flexibility essential to protein function, requiring solution state methods to describe the mechanisms underlying their function.^{35,36} We have therefore used NMR spectroscopy, small angle scattering and smFRET to characterize the behavior of avian 627-NLS in solution and its binding to importin α .

NMR unambiguously detects large-scale conformational changes of 627-NLS in solution, comprising exchange between a closed form and a previously uncharacterized open state that is highly dynamic. The chemical shifts of the open state very closely resemble the independent domains, indicating that the domains evolve more or less independently of each other in solution, sampling multiple conformational states with characteristic exchange time scales faster than $50 \mu\text{s}$. The two domains are separated by a short 12–14 amino acid linker that is partially structured in the closed state, participating in the electrostatic interaction that stabilizes the closed form, but that becomes flexible in the open state, providing the degrees of freedom necessary for the large-scale domain dynamics. Mutation of one of the highly conserved amino acids that constitutes the core of the stabilizing interaction results in a conformational equilibrium comprising only the open-state equilibrium, as demonstrated by both NMR and smFRET.

Exchange between the open and closed forms of 627-NLS occurs on a very slow time scale ($k_{\text{ex}} = 30 \text{ s}^{-1}$ at $15 \text{ }^\circ\text{C}$), exhibiting clear temperature dependence, rising to 80 s^{-1} at $25 \text{ }^\circ\text{C}$. Equally importantly, the population of the open state is strongly temperature-dependent, characterized by a predominantly closed form at $5 \text{ }^\circ\text{C}$ (20%:80% open:closed population) with population of the open form rising to approximately 50% at $30 \text{ }^\circ\text{C}$. NMR exchange and small angle scattering measured over a physiological range concord very closely with this description. A precise investigation of the thermodynamics governing the temperature-dependent equilibrium, derived from simultaneous analysis of CEST as a function of temperature, indicates that although enthalpic differences dominate the activation energy, the free form exhibits both entropic and enthalpic contributions compared to the closed state, suggesting that the open state may exhibit nonspecific nonbonding interactions between the surfaces.

The unambiguous identification of interconversion time-ranges within the open state ($\tau_{\text{ex}} < 50 \mu\text{s}$) and between the open and the closed states ($\tau_{\text{ex}} > 20 \text{ms}$) provides a clear framework within which smFRET can be used to probe the distance distributions between chromophores present in the two domains. This allows us to support the suggestion that the closed state indeed corresponds to the crystal conformation, and identifies significant domain dynamics in the open state, again in agreement with the model derived from NMR and SAXS.

Solution state approaches were also used to probe the interactions with importin $\alpha 1$, demonstrating that the 627 domain is detached from the NLS domain in the complex, sampling conformations in the vicinity of the C-terminus of importin α . The 627 domain clearly does not sample all of the available space provided by the flexible linker, possibly due to interactions with the surface of importin α in this region, or via interactions with the 34 amino acid long flexible C-terminal tail of importin α . This domain clearly remains flexible when the NLS domain is bound to importin as shown from both SAXS and smFRET. We note that the C-terminal tail of importin α presents a highly conserved acidic strand at its N-terminus, and a conserved cluster of aromatic moieties at its C-terminus,³⁷ which may interact with the surface of 627. The smFRET results suggest that the population of the closed state of 627-NLS is reduced to very low levels in complex with importin α , corroborating the model by which the open state is the binding competent form. Experiments carried out on four importin α isoforms ($\alpha 1$, $\alpha 3$, $\alpha 5$, and $\alpha 7$) indicate that this mechanism is general for PB2 binding to all members of the importin α family.

A recent study of residues involved in enhanced polymerase activity in 627-NLS found that mutation of the basic 650 residue, an essential constituent of the stabilizing salt bridge, resulted in efficient nuclear import but reported a lack of polymerase activity in the nucleus.³⁸ This supports our observation that the open form mediates interaction with importin α , and further supports the recent observation that the closed form is essential for function within the context of the reconstituted polymerase-RNA complex, where it has been proposed to play a crucial role in interaction with transcribed RNA in the polymerase exit tunnel.¹⁰

Although NMR exchange experiments comparing the avian and human forms were not able to detect any significant difference in the thermodynamics of the equilibrium, it is possible that the thermodynamic dependence of the solution state equilibrium of 627-NLS is related to temperature adaptation from the warmer environment of the bird intestine (40 °C) to the cooler mammalian respiratory tract (33 °C). Further studies are required to substantiate this possibility.

CONCLUSION

A combination of complementary solution-state approaches reporting on local and long-range protein dynamics is used to characterize the conformational behavior of the C-terminal 627-NLS domain of influenza polymerase PB2. Although in the crystalline form 627-NLS systematically adopts a closed, compact conformation, in solution the protein samples a dynamic equilibrium between the closed state and an open state, in which the two domains dislocate when a highly conserved tripartite salt bridge in the 627-NLS interface is ruptured. The open state is highly dynamic, comprising independent domains joined by the linker that also becomes

flexible. Open and closed states are present in equilibrium in slow exchange, with the open-state population, and the exchange rate, both increasing with temperature. Crucially only the open-form is capable of binding to the nuclear import receptor, and upon binding the 627 domain samples a dynamic conformational equilibrium in the vicinity of the C-terminus of importin α . This study demonstrates the functional importance of large-scale domain dynamics, mediated by the intrinsically disordered linker peptide connecting the two domains, and thereby provides a framework for understanding nuclear import of influenza polymerase. In particular we observe that the interaction of PB2 with importin α likely occurs via conformational selection from the intrinsic pre-existing equilibrium, rather than induced fit. More generally, this study provides a fascinating example of how a combination of solution-state approaches can precisely report on dynamic conformational equilibria, and as such offer the possibility to study the function of proteins exhibiting extensive and functionally important domain dynamics.^{39,40}

METHODS

Protein Expression and Purification. Codon-optimized *pb2* synthetic genes were synthesized encoding amino acids 538–759 (627-NLS domain) from human H3N2 A/Victoria/3/1975 and avian H5N1 A/duck/Shantou/4610/2003 for optimal expression in *E. coli* (Genentech, Regensburg, Germany). Two additional PB2 constructs from both human H3N2 A/Victoria/3/1975 and avian H5N1 A/duck/Shantou/4610/2003 were used: the 627 domain, aa 538–693 and the NLS domain, aa 678–759. The human importin- $\alpha 1$ isoform lacking the autoinhibitory N-terminal importin- β -binding domain, but with native C-terminus (KPNA2; Uniprot P52292, aa 60–529) was also expressed from a synthetic gene as above. All constructs were subcloned into a pET9a-derived vector with an N-terminal hexahistidine tag and TEV protease cleavage sequence (MGHHH-HHHHDYDIPTTENLYFQG).

The plasmids were transformed into *E. coli* BL21(DE3)RIL cells (Agilent), and the expression of the recombinant proteins was induced with 1 mM isopropyl-1-thio- β -D-galactopyranoside (IPTG) for 18 h at 16 °C. Cells were harvested by centrifugation, suspended in buffer A (50 mM Tris-HCl, 200 mM NaCl), pH 7.5, containing protease inhibitors (Complete EDTA-Free, Roche Diagnostics) and disrupted by sonication. The extract was centrifuged at 20000g for 30 min at 4 °C. All proteins were purified by affinity chromatography on a Ni²⁺ resin column (Qiagen) followed by incubation with TEV protease overnight at 4 °C coupled with a dialysis against buffer A, pH 7. A second affinity chromatography on a Ni²⁺ resin column was performed. The flow-through was then further purified using SEC with a Superdex S75 column (GE Healthcare) equilibrated in buffer A at pH 6.5.

Samples for NMR spectroscopy were produced in M9 minimal medium containing MEM vitamins (Gibco). For producing ¹⁵N-labeled or ¹⁵N,¹³C-labeled 627-NLS, 627, and NLS domains, the medium was supplemented with 1.0 g/L of ¹⁵NH₄Cl and 2.0 g/L of unlabeled glucose or 1.0 g/L of ¹⁵NH₄Cl and 2.0 g/L of ¹³C-glucose, while for producing ¹⁵N,¹³C,²H-labeled 627-NLS, the minimal medium was prepared in D₂O and supplemented with 1.0 g/L of ¹⁵NH₄Cl and 2.0 g/L of deuterated ¹³C-glucose. The purity and monodispersity of the samples were checked by SDS-PAGE, dynamic light scattering, and mass spectrometry.

The avian 627-NLS:human importin $\alpha 1$ complex was obtained by mixing both purified proteins in a ratio 1.5:1. Because SAXS experiments require a very high quality sample in terms of monodispersity, the obtained complex was further purified using SEC on Superdex 75 (GE Healthcare) equilibrated with 50 mM Tris-HCl, pH 6.5, 200 mM NaCl, and the subsequent sample was ultracentrifuged at 50000g during 20 min. The quality of the sample

containing the complex and the monodispersity were assessed by SDS-PAGE and dynamic light scattering, respectively.

Mutants of avian 627-NLS were made using the QuikChange site-directed mutagenesis kit (Agilent). A single mutant (R650A) was made for NMR measurements of the open conformation of 627-NLS, a double mutant I539C/A707C and a triple mutant R650A/I539C/A707C were made for smFRET measurements. All mutants were expressed and purified as described above for the wild-type protein. For the cysteine mutations, 10 mM dithiothreitol (DTT) was added after the second Ni-NTA column to keep the proteins in a monomeric state until labeling them for smFRET.

Structure Determination of the Avian 627-NLS Domain.

Hanging drop vapor diffusion trials were carried out at 20 °C. Native crystals of avian 627-NLS were obtained by mixing 1 μ L of protein solution at 12 mg/mL in 20 mM HEPES (pH 7.5), 200 mM NaCl, with an equal volume of a solution containing 0.1 M Bis-Tris (pH 6.5), 30% (w/v) PEG 4000, and 0.08 M magnesium acetate tetrahydrate. Crystals were washed in crystallization solution supplemented with 30% glycerol and frozen in liquid nitrogen.

Data were collected to 1.4 Å resolution on beamline BM14 at the European Synchrotron Radiation Facility (ESRF). All data collection and refinement statistics are given in Table S6. All data were integrated with XDS⁴¹ and analyzed using the CCP4i package.⁴² The structure was determined by molecular replacement using PHASER⁴³ with the human PB2 627-NLS domain (PDB 2VY6) as search model. ARP/wARP⁴⁴ was used for automatic model building. All refinements were performed with REFMAC.⁴⁵ According to MOLPROBITY (<http://molprobity.biochem.duke.edu/>), all structures have excellent geometry.

NMR Measurements. All samples for NMR contained 50 mM Tris-HCl pH 6.5, 200 mM NaCl, and 10% D₂O. The assignment of the avian NLS domain was obtained at 25 °C using a ¹⁵N,¹³C-labeled sample (1.0 mM) using BEST-type triple-resonance experiments⁴⁶ recorded on a Varian spectrometer operating at a ¹H frequency of 600 MHz, equipped with a cryoprobe. The assignment of the avian 627 domain was obtained at 25 °C using a ¹⁵N,¹³C-labeled sample (0.66 mM) using standard triple-resonance experiments recorded on a Varian spectrometer operating at a ¹H frequency of 800 MHz, equipped with cryoprobe.

The assignment of the avian 627-NLS domain was obtained at 10 °C using a ¹⁵N,¹³C,²H-labeled sample (0.5 mM) using BEST-TROSY triple-resonance experiments⁴⁷ recorded on a Bruker spectrometer operating at a ¹H frequency of 950 MHz. The assignment of 627-NLS was carried out at 10 °C to minimize line broadening due to exchange between open and closed conformations. The assignment of the R560A mutant of the avian 627-NLS domain was obtained at 10 °C using a ¹⁵N,¹³C-labeled sample (2.0 mM) using BEST-TROSY triple-resonance experiments recorded on a Bruker spectrometer operating at a ¹H frequency of 950 MHz. For all four proteins the spectra were processed in NMRPipe,⁴⁸ manually peak-picked in Sparky,⁴⁹ and MARS⁵⁰ was used for identification of spin systems followed by manual verification.

The evolution of the spectra with temperature was investigated by performing a series of ¹H–¹⁵N TROSY (627-NLS) or ¹H–¹⁵N HSQC (627 and NLS) spectra at 5, 10, 15, 20, 25, 30, and 35 °C. Intensities of the resonances corresponding to the open and closed conformations of 627-NLS were obtained by a line shape analysis (Lorentzian) at each temperature using the program FuDa (<http://www.biochem.ucl.ac.uk/hansen/fuda/>). The populations of the open and closed forms at each temperature were calculated from the extracted intensities.

CEST experiments²¹ were performed on a sample of 627-NLS (0.8 mM) at 5, 10, 15, and 20 °C on a Bruker spectrometer operating at a ¹H frequency of 700 MHz. The experiments were recorded with a ¹⁵N B₁ saturating field of 22 Hz (5, 10, 15, and 20 °C) and an additional CEST experiment was recorded at 10 °C using a B₁ field of 44 Hz. The B₁ field was applied during a constant period of 0.3 s. The experiments were recorded with 84 two-dimensional planes with the position of the ¹⁵N B₁ field ranging from 100 to 136 ppm in steps of 30 Hz. The CEST data were analyzed using ChemEx assuming a two-

site exchange model. To increase the robustness of the analysis of the CEST experiments, data at 5, 10, 15, and 20 °C were analyzed simultaneously assuming an Eyring relationship,

$$k = \frac{k_{\text{B}}T}{h} \exp\left(-\frac{\Delta H - T\Delta S}{RT}\right) \quad (1)$$

where k is the rate constant, ΔH (in J/mol) and ΔS (in J/mol/K) are the enthalpy and entropy of activation, respectively, k_{B} is the Boltzmann constant, h is Planck's constant, and R is the gas constant. Multiple resonances corresponding to the closed conformation of 627-NLS were included in the global fit (R650N, G651N, G682N, S688N, R692N, G693N, F694N, and I726N) at each temperature, and uncertainties in the entire fitting procedure were determined using 500 noise-based Monte Carlo simulations. The global fit of the CEST data thus characterizes the thermodynamic properties of the exchange process between the open and closed state of 627-NLS.

Nuclear relaxation rates of the 627-NLS R650A mutant were measured at 10 °C on a Bruker spectrometer operating at a ¹H frequency of 600 MHz. The ¹⁵N longitudinal relaxation rates (R_1) and ¹H-¹⁵N heteronuclear NOEs were measured using the methods of Lakomek et al.,⁵¹ the ¹⁵N transverse relaxation rates (R_2) were measured using the method of Kay et al.⁵² and the ¹⁵N–¹H CSA/DD cross-correlated transverse cross-relaxation rates (η_{xy}) were measured using the pulse scheme of Wang et al.⁵³ All spectra were processed in NMRPipe,⁴⁸ and in-house scripts were used to extract peak heights and calculate the relaxation rates.

Small-Angle X-ray Scattering of Avian 627-NLS.

SAXS experiments of avian 627-NLS were obtained at 5, 10, 20, 25, and 30 °C at the BM29 beamline, ESRF, Grenoble⁵⁴ using an energy of 12.5 keV, $\lambda = 0.9918$ Å. All samples were purified as described above. Fifty μ L of protein solution at three different concentrations (4.9, 2.45, and 1.23 mg/mL) and the corresponding buffers were exposed to X-rays and scattering data collected using the robotic sample handling available at the beamline.⁵⁵ Ten individual frames were collected for every exposure, each 1 s in duration using the Pilatus 1M detector (Dectris) placed 2.864 m from the sample. Individual frames were processed automatically and independently using the EDNA processing pipeline incorporating the ATSAS tools from EMBL-Hamburg, yielding individual radially averaged curves of normalized intensity versus scattering angle $q = 4\pi \sin \theta/\lambda$. Time frames were combined, excluding any data points affected by aggregation induced by radiation damage, to give the average scattering curve for each measurement (buffer was measured before and after every sample and averaged for background subtraction). Data were processed using the ATSAS package⁵⁶ and in-house software.

To analyze the experimental SAXS data of 627-NLS at the different temperatures, two different ensembles were created corresponding to the closed and open conformation of 627-NLS. For the “closed” ensemble, the crystal structure of avian 627-NLS (encompassing residues 541–741) was used and *flexible-meccano*^{22,23} was employed to add the flexible NLS peptide to the crystal structure assuming statistical coil distributions for these amino acids (residues 742–759). The “open” ensemble was generated as for the “closed” ensemble, but in addition the inter-domain linker between the 627 and the NLS domain 677–689) was also constructed using *flexible-meccano*, thereby obtaining an ensemble of structures where the 627 and the NLS domain are dislocated and can evolve freely within the limits of the conformational degrees of freedom allowed by the linker peptide. SAXS curves were predicted for each of the two ensembles (“open” and “closed”) by averaging predicted SAXS curves for individual structures over the entire ensembles. The two predicted SAXS curves were then combined in a population-weighted average using the populations of the open and closed conformations extracted from the line shape analysis of the TROSY spectra or the CEST experiments at the different temperatures. These population-weighted averages were then compared to the experimental SAXS curves at the different temperatures (Figure 6b,c).

Small-Angle X-ray Scattering of Avian 627-NLS in Complex with Human Importin α 1. SAXS experiments of the complex of avian 627-NLS and human importin α 1 were obtained at 5 °C at the

ID14-3 beamline, ESRF, Grenoble, which operated at a fixed energy (13.32 keV, $\lambda = 0.931 \text{ \AA}$). All samples were purified as described above and checked for monodispersity by dynamic light scattering. Aliquots of 30 μL of protein solution at three different concentrations (1, 0.5, and 0.2 mg/mL) for each sample (and buffer) were exposed to X-rays, and scattering data were collected using the robotic sample handling available at the beamline. Ten individual frames were collected for every exposure, each 30 s in duration using the Pilatus 1M detector (Dectris) placed 1.83 m from the sample. Individual frames were processed automatically and independently using the EDNA processing pipeline using the ATSAS tools from EMBL-Hamburg, yielding individual radially averaged curves of normalized intensity versus scattering angle $q = 4\pi \sin \theta/\lambda$. Time frames were combined, excluding any data points affected by aggregation induced by radiation damage, to give the average scattering curve for each measurement (buffer was measured before and after every sample and averaged for background subtraction). Data were processed and analysis steps were performed using the ATSAS package.⁵⁶ Forty *ab initio* models were calculated using DAMMIF,⁵⁷ and then averaged and aligned using DAMAVER.⁵⁸

In order to analyze the experimental SAXS curve of the avian 627-NLS:human importin $\alpha 1$ complex in more detail, an ensemble of structures was generated on the basis of the crystal structure of the human NLS domain in complex with importin $\alpha 1$.¹⁹ *Flexible-meccano* was used to construct the linker peptide between the NLS and the 627 domain providing an ensemble of structures of the 627-NLS:importin complex where the 627 domain samples a large number of conformations as allowed by statistical coil sampling of the linker peptide (Figure 7a). Compared to the available crystal coordinates, the experimental construct comprised 13 amino acids at the N terminus and 34 amino acids at the C terminus that are predicted to be disordered and were built using *flexible-meccano* (residues 60–72 and 496–529, respectively). For each structure of the generated ensemble, the SAXS curve was predicted and compared to the experimental scattering curve (Figure 7a). In addition, sub-ensembles of structures (of sizes ranging from 5 to 25) that agree with the experimental SAXS curve were selected from the entire 25 000 orientations represented in Figure 7a, using the genetic algorithm ASTEROIDS.^{59–61}

Small-Angle Neutron Scattering of Avian 627-NLS in Complex with Human Importin $\alpha 1$. SANS experiments of the complex of avian 627-NLS and human importin $\alpha 1$ were obtained at 8 °C at the D33 beamline, Institut Laue-Langevin (ILL), Grenoble. The neutron beam had a wavelength $\lambda = 6 \text{ \AA} \pm 10\%$, and was passed through a 2 or 14.4 m rectangular collimator. Sample-to-detector distances were 2 and 14 m. The q range covered in this experiment extended from 0.004 to 0.048 nm^{-1} . The complex, at 2.45 mg/mL in 100% D_2O buffer, and the corresponding buffer were measured in 2 mm thick rectangular cuvettes.

The SANS data were used to validate the SAXS-derived structure/ensemble of the 627-NLS:importin $\alpha 1$ complex. Thus, SANS curves were calculated using CRYSON²⁵ from (1) the best-fitting structure of the complex (Figure 7b) and (2) the ensemble sampling all possible conformations of 627 on the surface of the NLS:importin complex (Figure 7a). The calculated SANS curves for the three cases were subsequently compared to the experimental SANS data (Figure S5).

Single-Molecule FRET of 627-NLS. Double-cysteine mutants of 627-NLS were randomly labeled with Alexa488- and Alexa594-maleimide in a 1:1 ratio, following previously described protocols.²⁹ Briefly, the protein was buffer exchanged into 50 mM Tris pH 7, 200 mM NaCl with 10 mM DTT, and transferred quickly into DTT-free buffer prior to labeling. Free cysteines were labeled with a 3–5-fold molar excess of dye, with unincorporated dye being removed by size exclusion chromatography. The buffer was exchanged into 50 mM Tris pH 6.5, 200 mM NaCl, 2 mM DTT for single-molecule measurements.

The smFRET measurements were performed at 627-NLS concentrations of 50 pM on a custom-built multi-parameter fluorescence spectrometer with a confocal detection geometry, as described previously.⁶² A laser diode (LDH 485, Picoquant, Berlin, Germany) and a white light laser (SuperK Extreme, NKT Photonics,

Denmark) filtered through a 572/15 excitation filter were pulsed alternately with a repetition frequency of 27 MHz each to excite Alexa488 and Alexa594, respectively. Excitation light was linearly polarized. Fluorescence light was spatially filtered by a 100 μm pinhole, split into parallel and perpendicular polarized light, and then into Alexa488 (Do) and Alexa594 (Ac) fluorescence.

Fluorescence time traces were subjected to a burst recognition algorithm,⁶³ and all bursts with a Do+Ac intensity of more than 50 photons arising from excitation with the green laser were then further analyzed by multi-parameter analysis. FRET efficiencies (E_{FRET}) were calculated from fluorescence Do and Ac signals that were corrected for leakage and direct excitation according to

$$E_{\text{FRET}} = \frac{I_{\text{Ac}}}{I_{\text{Ac}} + \gamma I_{\text{Do}}} \quad (2)$$

with the correction for differences in detection efficiencies and quantum yields $\gamma = 1.14$. γ for 627-NLS was determined using established protocols.^{29,64} An independent validation of the measured γ can be obtained from considering the closed conformation of 627-NLS, which does not exhibit domain dynamics according to NMR and SAXS. For such a static molecule, γ can also be obtained from the following relationship:

$$E_{\text{FRET}} = \frac{I_{\text{Ac}}}{I_{\text{Ac}} + \gamma I_{\text{Do}}} = 1 - \frac{\tau_{\text{DA}}}{\tau_{\text{D}}} \quad (3)$$

with τ_{D} and τ_{DA} being the Do lifetimes in the absence and presence of an active Ac. Indeed, the closed conformation of 627-NLS follows this behavior with the γ used (Figure 9 and Figure S7).

Labeling stoichiometries (S) were calculated according to

$$S = \frac{I_{\text{Do}}}{I_{\text{Do}} + I_{\text{Ac}} + I_{\text{Ac}}^{\text{dir}}} \quad (4)$$

with $I_{\text{Ac}}^{\text{dir}}$ being the intensity of Ac arising from direct excitation with the Ac laser. In most cases (Figures S6 and S7, and all derived analyses), only bursts of $S = 0.2$ –1.2 were selected for further analysis.²⁸

Fluorescence lifetimes were fit using a maximum likelihood estimator.⁶⁵ E and τ were then plotted in two-dimensional histograms and fit with double ($x = 1$) or triple ($x = 2$) Gaussian functions according to

$$f(E, \tau) = \sum_{n=0}^x A_n \exp \left[-\frac{1}{2(1-c_n^2)} \times \left(\left(\frac{E - E_n}{\sigma_{E,n}} \right)^2 + \left(\frac{\tau - \tau_n}{\sigma_{\tau,n}} \right)^2 - \frac{2c_n(E - E_n)(\tau - \tau_n)}{\sigma_{E,n}\sigma_{\tau,n}} \right) \right] \quad (5)$$

with the widths of the populations σ , and the centers E_n and τ_n . The parameter c describes a tilt of the Gaussian fit in the τ - E plane and was set to 0 when $x = 2$ was selected, unless noted otherwise.

Single-molecule lifetime fits yielding $\tau < 500$ ps arose from background bursts, as could be shown by more restrictive burst recognition parameters, and were excluded from consideration when triple Gaussian fits were attempted.

Three different approaches were taken up to analyze the presence of slow dynamics within the 627-NLS FRET histograms:

- FRET peaks resulting from a titration of 627-NLS I539C A707C with importin $\alpha 1$ were first fit with two two-dimensional Gaussian functions, allowing a tilt in the τ versus E_{FRET} histogram ($x = 1$ and $c_n \neq 0$ in the fitting equation). The peak widths of the FRET populations (σ_1 in the fitting equation, corresponding to σ_E in Table S4) were then compared with the widths as expected from a shot-noise (sn)-limited FRET peak according to

$$\sigma_{\text{sn}} = \frac{\sqrt{\langle E_{\text{FRET}}^m \rangle (1 - \langle E_{\text{FRET}}^m \rangle) (N^{-1})}}{\sqrt{\langle E_{\text{FRET}}^m \rangle (1 - \langle E_{\text{FRET}}^m \rangle) N_T^{-1}}} \quad (6)$$

where $\langle N \rangle$ is the average number of photons per burst and N_T the minimum number of photons per burst, corresponding to the threshold applied. $\langle E_{\text{FRET}}^m \rangle$ is the average FRET efficiency without γ correction.^{30,66} N_T was used for a conservative approximation of σ_{sn} . σ_1 that were significantly larger than σ_{sn} (as was the case throughout the whole importin $\alpha 1$ titration of 627-NLS, but particularly for 627-NLS alone and with low concentrations of the transport receptor) were indicative of slow dynamics of the dye-to-dye distance or the existence of multiple overlaid populations.^{30,66}

- (b) A tilt between E_{FRET} and τ within the FRET population of 627-NLS I539C A707C was necessary to reasonably fit the two-dimensional histograms with a double Gaussian ($x = 1$) population. However, for folded proteins with a clearly defined dye-to-dye distance, and for fast-fluctuating dye-to-dye distance distributions (much faster than inter-photon times, $\sim 50 \mu\text{s}$ in our case), no tilt would be expected within the same population in the E_{FRET} vs τ histogram.^{30,32,66}
- (c) Analyses considering different single-molecule observation times (binning analysis, Figure S6, shown for 0.5, 1, and 2 ms as well as resulting from burst recognition, i.e., up to ~ 5 ms) that yield similar peak widths and FRET positions are indicative of dynamics that are considerably slower than the time of a burst, or for two/several static molecules contributing to the observed FRET populations. Note that fast dynamics ($< \mu\text{s}$) are not covered by this analysis and can still be present.³²

Approaches (a)–(c) all point toward the existence of very slowly (> 5 ms) interconverting states, or static states contributing to the widths of the FRET histogram. The exchange rate between open and closed conformations in the unbound 627-NLS was estimated to be 50 s^{-1} at $25 \text{ }^\circ\text{C}$ by NMR. Fast interconversion rates within the open population of 627-NLS were found to be smaller than $\sim 10 \mu\text{s}$, whereas the closed population appears devoid of significant inter-domain fluctuations. All dynamics observed by NMR were therefore shorter than the inter-photon time ($\sim 50 \mu\text{s}$), or much longer than the observation time (up to ~ 5 ms), which suggests that a triple Gaussian function ($x = 2$, Figure S7c), without allowing tilt between τ and E_{FRET} within the same population ($c_n = 0$), should describe the two-dimensional τ versus E_{FRET} histograms reasonably well, which is indeed the case. However, in case small amounts of microsecond to millisecond time scale dynamics were present, we also allowed $c_n \neq 0$ in the fit. Under this scenario we determined FRET efficiencies for the open and closed forms, and both methods of fitting three Gaussian populations gave rise to the observation that the closed form was on the static E_{FRET} line, whereas the open form showed fast dynamics, leading to a deviation from the static FRET line (Figure S7d, Table S5).^{31,32} Additionally, both approaches yield a similar occupancy ratio between open and closed conformations to that found by NMR.

While determining distances for FRET populations that are dynamically averaged from a conformational ensemble requires the input of a specific model, the dye-to-dye distance R_{DA} for the closed, static, conformation could be calculated using

$$E_{\text{FRET}} = 1 / (1 + (R_{\text{DA}}/R_0)^6) \quad (7)$$

The Förster distance R_0 was determined using quantum yields and the overlap integral determined from singly labeled 627-NLS to be $58 \pm 1 \text{ \AA}$.²⁸

■ ASSOCIATED CONTENT

Supporting Information

The Supporting Information is available free of charge on the ACS Publications website at DOI: 10.1021/jacs.5b07765.

Tables S1–S3, chemical shift assignments; Tables S4 and S5, FRET peak widths, E_{FRET} , and τ for titration of 627-NLS with importin $\alpha 1$; Table S6, crystallographic data collection and refinement statistic of avian 627-NLS (S38–759); Figures S1–S4, showing chemical shift differences between open and closed forms of 627-NLS, NMR spectra of 627, NLS, and 627-NLS, sequence comparison, NMR relaxation data, and all CEST data and fits; Figure S5, reproduction of SANS data; and Figures S6–S8, showing analysis of FRET data of 627-NLS alone and in complex with importins $\alpha 1$, $\alpha 3$, $\alpha 5$, and $\alpha 7$ (PDF)

■ AUTHOR INFORMATION

Corresponding Authors

*hart@embl.fr

*martin.blackledge@ibs.fr

Notes

The authors declare no competing financial interest.

■ ACKNOWLEDGMENTS

This work was funded by the Agence Nationale de Recherche under ComplexDynamics (SIMI7, M.B.). S.M. acknowledges funding from an EMBO long-term fellowship. N.S. acknowledges funding from a Swiss National Science Foundation Early Postdoc Mobility Fellowship (P2ELP2 148858). E.D. acknowledges funding from the Région Rhône-Alpes. D.B. and S.B. acknowledge funding from the FINOVI foundation. This work used the platforms of the Grenoble Instruct Center (ISBG: UMS 3518 CNRS-CEA-UJF-EMBL) with support from FRISBI (ANR-10-INSB-05-02) and GRAL (ANR-10-LABX-49-01) within the Grenoble Partnership for Structural Biology (PSB). The authors thank Dr. Frank Gabel (IBS) for insightful discussions and the ESRF and ILL for the provision of beamtime for these experiments and the support of the staff. Parts of the NMR experiments were carried out at the large-scale NMR facility in Frankfurt, Germany, through access provided by the bio-NMR network. The authors thank Dr. Frank Löhr and Dr. Christian Richter for support in this context. E.L. acknowledges funding from the Emmy Noether program of the DFG.

■ REFERENCES

- Ruigrok, R. W. H.; Crépin, T.; Hart, D. J.; Cusack, S. *Curr. Opin. Struct. Biol.* **2010**, *20*, 104–113.
- Arranz, R.; Coloma, R.; Chichón, F. J.; Conesa, J. J.; Carrascosa, J. L.; Valpuesta, J. M.; Ortín, J.; Martín-Benito, J. *Science* **2012**, *338*, 1634–1637.
- Resa-Infante, P.; Jorba, N.; Coloma, R.; Ortín, J. *RNA Biol.* **2011**, *8*, 207–215.
- Moeller, A.; Kirchdoerfer, R. N.; Potter, C. S.; Carragher, B.; Wilson, I. A. *Science* **2012**, *338*, 1631–1634.
- Fodor, E. *Acta Virol.* **2013**, *57*, 113–122.
- Tarendeau, F.; Boudet, J.; Guilligay, D.; Mas, P. J.; Bougault, C. M.; Boulo, S.; Baudin, F.; Ruigrok, R. W. H.; Daigle, N.; Ellenberg, J.; Cusack, S.; Simorre, J.-P.; Hart, D. J. *Nat. Struct. Mol. Biol.* **2007**, *14*, 229–233.
- Deng, T.; Engelhardt, O. G.; Thomas, B.; Akoulitchev, A. V.; Brownlee, G. G.; Fodor, E. *J. Virol.* **2006**, *80*, 11911–11919.
- Kuzuhara, T.; Kise, D.; Yoshida, H.; Horita, T.; Murazaki, Y.; Nishimura, A.; Echigo, N.; Utsunomiya, H.; Tsuge, H. *J. Biol. Chem.* **2009**, *284*, 6855–6860.
- Tarendeau, F.; Crepin, T.; Guilligay, D.; Ruigrok, R. W. H.; Cusack, S.; Hart, D. J. *PLoS Pathog.* **2008**, *4*, e1000136.

- (10) Pflug, A.; Guilligay, D.; Reich, S.; Cusack, S. *Nature* **2014**, *516*, 355–360.
- (11) Mehle, A.; Doudna, J. A. *Proc. Natl. Acad. Sci. U. S. A.* **2009**, *106*, 21312–21316.
- (12) Massin, P.; van der Werf, S.; Naffakh, N. *J. Virol.* **2001**, *75*, 5398–5404.
- (13) Gabriel, G.; Herwig, A.; Klenk, H.-D. *PLoS Pathog.* **2008**, *4*, e11.
- (14) Czudai-Matwich, V.; Otte, A.; Matrosovich, M.; Gabriel, G.; Klenk, H.-D. *J. Virol.* **2014**, *88*, 8735–8742.
- (15) Resa-Infante, P.; Jorba, N.; Zamarreño, N.; Fernández, Y.; Juárez, S.; Ortín, J. *PLoS One* **2008**, *3*, e3904.
- (16) Boivin, S.; Hart, D. J. *J. Biol. Chem.* **2011**, *286*, 10439–10448.
- (17) Yamada, S.; Hatta, M.; Staker, B. L.; Watanabe, S.; Imai, M.; Shinya, K.; Sakai-Tagawa, Y.; Ito, M.; Ozawa, M.; Watanabe, T.; Sakabe, S.; Li, C.; Kim, J. H.; Myler, P. J.; Phan, I.; Raymond, A.; Smith, E.; Stacy, R.; Nidom, C. A.; Lank, S. M.; Wiseman, R. W.; Bimber, B. N.; O'Connor, D. H.; Neumann, G.; Stewart, L. J.; Kawaoka, Y. *PLoS Pathog.* **2010**, *6*, e1001034.
- (18) Smith, E. R.; Begley, D. W.; Anderson, V.; Raymond, A. C.; Haffner, T. E.; Robinson, J. I.; Edwards, T. E.; Duncan, N.; Gerdtts, C. J.; Mixon, M. B.; Nollert, P.; Staker, B. L.; Stewart, L. J. *Acta Crystallogr., Sect. F: Struct. Biol. Cryst. Commun.* **2011**, *67*, 1015–1021.
- (19) Pumroy, R. A.; Ke, S.; Hart, D. J.; Zachariae, U.; Cingolani, G. *Structure* **2015**, *23*, 374–384.
- (20) Gabriel, G.; Fodor, E. *Curr. Top. Microbiol. Immunol.* **2014**, *385*, 35–60.
- (21) Vallurupalli, P.; Bouvignies, G.; Kay, L. E. *J. Am. Chem. Soc.* **2012**, *134*, 8148–8161.
- (22) Bernadó, P.; Blanchard, L.; Timmins, P.; Marion, D.; Ruigrok, R. W. H.; Blackledge, M. *Proc. Natl. Acad. Sci. U. S. A.* **2005**, *102*, 17002–17007.
- (23) Ozenne, V.; Bauer, F.; Salmon, L.; Huang, J.-R.; Jensen, M. R.; Segard, S.; Bernadó, P.; Charavay, C.; Blackledge, M. *Bioinformatics* **2012**, *28*, 1463–1470.
- (24) Svergun, D.; Barberato, C.; Koch, M. *J. Appl. Crystallogr.* **1995**, *28*, 768–773.
- (25) Svergun, D. I.; Richard, S.; Koch, M. H. J.; Sayers, Z.; Kuprin, S.; Zaccai, G. *Proc. Natl. Acad. Sci. U. S. A.* **1998**, *95*, 2267–2272.
- (26) Kim, H. S.; Gabel, F. *Acta Crystallogr., Sect. D: Biol. Crystallogr.* **2015**, *71*, 57–66.
- (27) Konarev, P. V.; Petoukhov, M. V.; Volkov, V. V.; Svergun, D. I. *J. Appl. Crystallogr.* **2006**, *39*, 277–286.
- (28) Sisamakris, E.; Valeri, A.; Kalinin, S.; Rothwell, P. J.; Seidel, C. A. M. *Methods Enzymol.* **2010**, *475*, 455–514.
- (29) Milles, S.; Tyagi, S.; Banterle, N.; Koehler, C.; VanDelinder, V.; Plass, T.; Neal, A. P.; Lemke, E. A. *J. Am. Chem. Soc.* **2012**, *134*, 5187–5195.
- (30) Merchant, K. A.; Best, R. B.; Louis, J. M.; Gopich, I. V.; Eaton, W. A. *Proc. Natl. Acad. Sci. U. S. A.* **2007**, *104*, 1528–1533.
- (31) Kalinin, S.; Valeri, A.; Antonik, M.; Felekyan, S.; Seidel, C. A. M. *J. Phys. Chem. B* **2010**, *114*, 7983–7995.
- (32) Gopich, I. V.; Szabo, A. *Proc. Natl. Acad. Sci. U. S. A.* **2012**, *109*, 7747–7752.
- (33) Soranno, A.; Buchli, B.; Nettels, D.; Cheng, R. R.; Müller-Spätth, S.; Pfeil, S. H.; Hoffmann, A.; Lipman, E. A.; Makarov, D. E.; Schuler, B. *Proc. Natl. Acad. Sci. U. S. A.* **2012**, *109*, 17800–17806.
- (34) Vogel, C.; Bashton, M.; Kerrison, N. D.; Chothia, C.; Teichmann, S. A. *Curr. Opin. Struct. Biol.* **2004**, *14*, 208–216.
- (35) Ma, B.; Tsai, C.-J.; Haliloglu, T.; Nussinov, R. *Structure* **2011**, *19*, 907–917.
- (36) Huang, J.-R.; Warner, L. R.; Sanchez, C.; Gabel, F.; Madl, T.; Mackereth, C. D.; Sattler, M.; Blackledge, M. *J. Am. Chem. Soc.* **2014**, *136*, 7068–7076.
- (37) Chang, C.-W.; Couñago, R. L. M.; Williams, S. J.; Bodén, M.; Kobe, B. *Plant Cell* **2012**, *24*, 5074–5088.
- (38) Kirui, J.; Bucci, M. D.; Poole, D. S.; Mehle, A. *J. Virol.* **2014**, *88*, 5977–5986.
- (39) Bernadó, P.; Blackledge, M. *Nature* **2010**, *468*, 1046–1048.
- (40) Mackereth, C. D.; Sattler, M. *Curr. Opin. Struct. Biol.* **2012**, *22*, 287–296.
- (41) Kabsch, W. *J. Appl. Crystallogr.* **1993**, *26*, 795–800.
- (42) Collaborative Computational Project, Number 4. *Acta Crystallogr., Sect. D: Biol. Crystallogr.* **1994**, *50*, 760–763.
- (43) Read, R. J. *Acta Crystallogr., Sect. D: Biol. Crystallogr.* **2001**, *57*, 1373–1382.
- (44) Perrakis, A.; Morris, R.; Lamzin, V. S. *Nat. Struct. Biol.* **1999**, *6*, 458–463.
- (45) Murshudov, G. N.; Vagin, A. A.; Dodson, E. J. *Acta Crystallogr., Sect. D: Biol. Crystallogr.* **1997**, *53*, 240–255.
- (46) Lescop, E.; Schanda, P.; Brutscher, B. *J. Magn. Reson.* **2007**, *187*, 163–169.
- (47) Solyom, Z.; Schwarten, M.; Geist, L.; Konrat, R.; Willbold, D.; Brutscher, B. *J. Biomol. NMR* **2013**, *55*, 311–321.
- (48) Delaglio, F.; Grzesiek, S.; Vuister, G. W.; Zhu, G.; Pfeifer, J.; Bax, A. *J. Biomol. NMR* **1995**, *6*, 277–293.
- (49) Goddard, T. D.; Kneller, D. G. SPARKY; University of California, San Francisco, 2003.
- (50) Jung, Y.-S.; Zweckstetter, M. *J. Biomol. NMR* **2004**, *30*, 11–23.
- (51) Lakomek, N.-A.; Ying, J.; Bax, A. *J. Biomol. NMR* **2012**, *53*, 209–221.
- (52) Kay, L. E.; Torchia, D. A.; Bax, A. *Biochemistry* **1989**, *28*, 8972–8979.
- (53) Wang, C.; Rance, M.; Palmer, A. G. *J. Am. Chem. Soc.* **2003**, *125*, 8968–8969.
- (54) Pernot, P.; Theveneau, P.; Giraud, T.; Fernandes, R. N.; Nurizzo, D.; Spruce, D.; Surr, J.; McSweeney, S.; Round, A.; Felisaz, F.; Foedinger, L.; Gobbo, A.; Huet, J.; Villard, C.; Cipriani, F. *J. Phys. Conf. Ser.* **2010**, *247*, 012009.
- (55) Round, A. R.; Franke, D.; Moritz, S.; Huchler, R.; Fritsche, M.; Malthan, D.; Klaering, R.; Svergun, D. I.; Roessle, M. *J. Appl. Crystallogr.* **2008**, *41*, 913–917.
- (56) Petoukhov, M. V.; Franke, D.; Shkumatov, A. V.; Tria, G.; Kikhney, A. G.; Gajda, M.; Gorba, C.; Mertens, H. D. T.; Konarev, P. V.; Svergun, D. I. *J. Appl. Crystallogr.* **2012**, *45*, 342.
- (57) Franke, D.; Svergun, D. I. *J. Appl. Crystallogr.* **2009**, *42*, 342–350.
- (58) Volkov, V. V.; Svergun, D. I. *J. Appl. Crystallogr.* **2003**, *36*, 860–864.
- (59) Nodet, G.; Salmon, L.; Ozenne, V.; Meier, S.; Jensen, M. R.; Blackledge, M. *J. Am. Chem. Soc.* **2009**, *131*, 17908–17918.
- (60) Salmon, L.; Nodet, G.; Ozenne, V.; Yin, G.; Jensen, M. R.; Zweckstetter, M.; Blackledge, M. *J. Am. Chem. Soc.* **2010**, *132*, 8407–8418.
- (61) Jensen, M. R.; Zweckstetter, M.; Huang, J.; Blackledge, M. *Chem. Rev.* **2014**, *114*, 6632–6660.
- (62) Milles, S.; Lemke, E. A. *Biophys. J.* **2011**, *101*, 1710–1719.
- (63) Eggeling, C.; Berger, S.; Brand, L.; Fries, J. R.; Schaffer, J.; Volkmer, A.; Seidel, C. A. *J. Biotechnol.* **2001**, *86*, 163–180.
- (64) Ferreon, A. C. M.; Gambin, Y.; Lemke, E. A.; Deniz, A. A. *Proc. Natl. Acad. Sci. U. S. A.* **2009**, *106*, 5645–5650.
- (65) Schaffer, J.; Volkmer, A.; Eggeling, C.; Subramaniam, V.; Striker, G.; Seidel, C. A. M. *J. Phys. Chem. A* **1999**, *103*, 331–336.
- (66) Gopich, I.; Szabo, A. *J. Chem. Phys.* **2005**, *122*, 014707.
- (67) Marsh, J. A.; Singh, V. K.; Jia, Z.; Forman-Kay, J. D. *Protein Sci.* **2006**, *15*, 2795–2804.
- (68) Maltsev, A. S.; Ying, J.; Bax, A. *J. Biomol. NMR* **2012**, *54*, 181–191.